

# A Small All-Corners-Truncated Circularly Polarized Microstrip Patch Antenna on Textile Substrate for Wearable Passive UHF RFID Tags

Duc Le, *Student Member, IEEE*, Shahbaz Ahmed, *Student Member, IEEE*, Leena Ukkonen, *Member, IEEE*, Toni Björninen, *Senior Member, IEEE*

**Abstract**—We present a wearable passive UHF RFID tag based on a circularly polarized (CP) patch antenna on a textile substrate. The antenna miniaturization is based on applying a combination of the cross- and L-shaped slots in the radiator. In conjunction, the right-hand circular polarization is achieved by asymmetrically truncating all four corners of the square-shaped radiator. Despite using a regular low-permittivity textile as the antenna substrate, we downsized the antenna to a  $5\text{ cm} \times 5\text{ cm}$  footprint with the thickness of 4 mm, which is equal to  $0.1525\lambda \times 0.1525\lambda \times 0.0091\lambda$ , where  $\lambda$  is the free space wavelength at 915 MHz. In the numerical modeling and optimization of the antenna, we used a simplified cuboid-shaped and anatomical human body models. In addition to simulated conventional antenna performance indicators, we introduce spatial coverage as a new parameter for assessing the detection reliability of UHF RFID tags. Finally, we measured a manufactured tag worn in four different configurations on the body. The measured axial ratio value was approximately 2 dB in all cases and the tag provided a high attainable read range of around 5.8 meters for a right-hand CP reader emitting 3.28 W EIRP.

**Index Terms**—Wearable antenna, circular polarization, passive UHF RFID tag, wearable RFID tag, wireless body-area systems.

## I. INTRODUCTION

Microwave and antenna technology has become widely applied in wireless body area systems [1-4]. Here the versatile and energy- and cost-efficient passive ultra-high frequency (UHF) radio-frequency identification (RFID) technology and RFID-inspired backscattering communications and sensing systems have been recognized as a compelling approach. The relevant applications range from identification, access control, and localization to wireless health, including wearable and implantable devices [5-7]. The two fundamental challenges related to wearable antennas are the mitigation of the negative impact arising from the electromagnetic (EM) interaction between the antenna and the dissipative biological tissue and applying textile materials and compatible manufacturing methods to achieve practical cloth-integration of antennas.

In the most of the commercial domain UHF RFID systems deployed for item-level tracking, tags comprise miniaturized dipole antennas, which are inherently linearly polarized [8], but single-layer CP tag antennas have also been studied [9][10][11][12]. However, due to the well-known miniaturization methods available for the dipole antennas and the cost-efficient mass production of the single-layer label-type dipole tags [13][14], they remain the most common type of antennas for UHF RFID tags. Under this paradigm, the reader antennas are normally CP for avoiding the chance of cross-polarization [8] with linearly polarized tags. In contrast, in wireless body area systems where the unavoidable antenna-body EM coupling limits the performance and robustness of single-layer antennas [15][16], structures including a ground plane or other types of decoupling metallic structures are preferred. This approach has been used to create well-performing textile-based  $50\text{-}\Omega$ -matched wearable CP antennas at mid- and high-UHF frequencies, e.g. GPS and 2.4 GHz ISM band applications [17][18][19]. Recently, also the development of wearable CP antennas for UHF RFID tags operating in the lower UHF band (866/915 MHz) has been gaining attention [20][21]. This provides a new alternative for the wireless body-area UHF RFID systems by improving the polarization efficiency and thereby the tag's peak read range and detection reliability.

In our previous work [21], we studied a CP microstrip patch antenna for a wearable passive UHF RFID tag attached to the upper back of a person. In this article, we report a new wearable CP patch antenna for wearable tags along with numerous other advancements, including more accurate numerical models, a more accurate measurement technique and a practical evaluation of the robustness of the tag's performance when placed at various locations on body.

For the numerical modeling, we have used realistically sized simplified cuboid-shaped and anatomical human body models. Regarding the antenna structure, by truncating all four corners of the radiating patch asymmetrically, in contrast to two in [21], allowed us to completely remove the inductive matching loop

structure from the antenna and avoid the narrow traces included in the radiating patch in [21]. This maximized the size of the radiating patch without increasing the size of the antenna for enhanced EM performance and improved the tag's structural durability. In the numerical analysis, we introduce spatial coverage as a new parameter for assessing the detection reliability of UHF RFID tags. For the wireless testing of the fully assembled prototype tag, we have formulated and implemented a new improved approach to measuring the tag antenna's axial ratio and the attainable read range of the tag for a CP reader antenna. Finally, as a crucial practical aspect, we studied the robustness of the tag by measuring it at various locations on the body and with different clothing thickness to prove its applicability for wearable systems.

## II. TAG ANTENNA STRUCTURE, NUMERICAL MODELING, AND PERFORMANCE EVALUATION

### A. Numerical Modeling

We used ANSYS High-Frequency Structure Simulator (HFSS) with a full-wave electromagnetic field solver based on the finite element method in modeling and optimization of the antenna. The optimization target was to obtain the frequency of the minimum axial ratio and peak read range at 915 MHz by tuning the L-slots' length and the truncation of the four corners of the radiating patch. Fig. 1 demonstrates the geometry of the antenna in detail with side and front views. As shown in Fig. 1, the UHF RFID microchip (NXP UCODE G2iL; turn-on power  $-18$  dBm) was attached on the vertical wall of the substrate. In the numerical modeling, we used the parallel connection of the resistance  $R = 2850 \Omega$  and capacitance  $C = 0.91$  pF as an equivalent circuit giving the frequency-dependent impedance for the microchip [22]. At 915 MHz the impedance is  $12.8 - j191 \Omega$ . The total size of the antenna is  $5 \text{ cm} \times 5 \text{ cm}$  with the thickness of 4 mm, which is equal to  $0.1525\lambda \times 0.1525\lambda \times 0.0091\lambda$ , where  $\lambda$  is the free space wavelength at 915 MHz. With this small size, the antenna can be readily worn on various parts of the body, for instance, arm, thigh, and back. As compared with [20], in this work, we totally removed the inductive matching loop from the antenna to increase space for the signal plane and simplify the fabrication process. The four truncated corners (parameters  $i$ ,  $k$ ,  $g$  and  $h$  in Fig. 1) and the spacing between the L-shaped slots (parameter  $x$  in Fig. 1) played the key role in optimizing the axial ratio at 915 MHz.

The miniaturization of the antenna was achieved by combining the cross slots cutting the radiating patch diagonally and the four L-shaped slots; a technique proposed in [23] for a  $50\text{-}\Omega$ -matched two-corners truncated patch on a high-permittivity microwave laminate as the substrate and superstrate. The slots modify the distribution of the surface current density on the radiating patch in a strategic way, such that the resonance frequency of the antenna is considerably lowered while the radiation efficiency is reduced proportionally much less [23]. Our antenna does not include a superstrate and the substrate material we used was low-permittivity ethylene propylene diene monomer (EPDM) foam ( $\epsilon_r = 1.53$ ,  $\tan\delta = 0.02$  at 915 MHz [24]), which was sandwiched between the ground

plane and radiating patch. The conductors are made of  $40\text{-}\mu\text{m}$  copper foil (conductivity: 58 MS/m). Following the antenna self-matching principle commonly applied in RFID tag antennas to avoid lumped component matching circuits between the antenna and the microchip, we adjusted the distance between the middle of the antenna and the shorting pin (parameter  $e$  in Fig. 1).

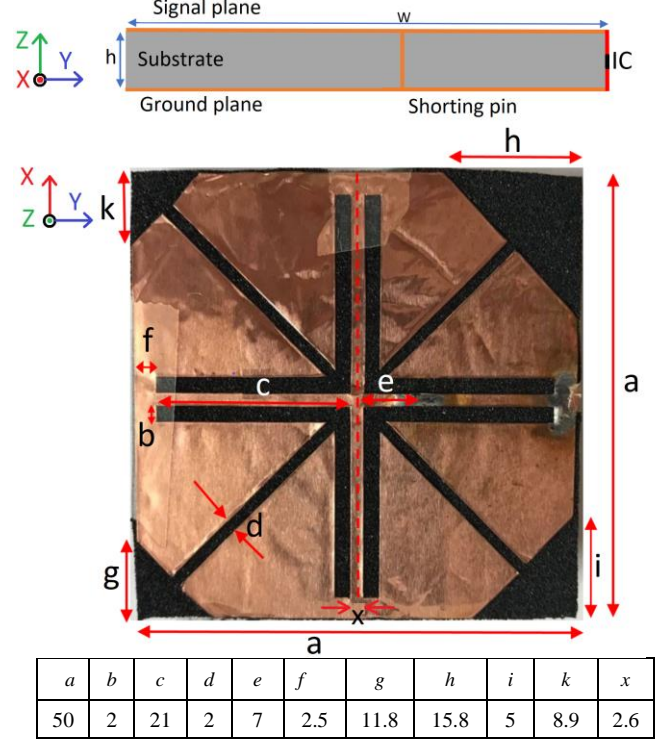


Fig. 1. The side view of the tag (top) and the top view (bottom) with the geometrical parameters reported in millimeters.

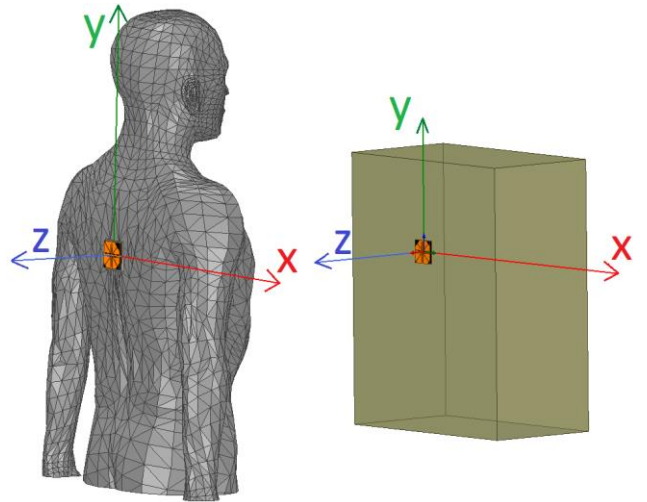


Fig. 2. The anatomical model (left side) and the cuboid model (right side).

To account for the impact of the person wearing the tag on the electromagnetic properties of the antenna, we modelled the antenna on two different body models in our numerical simulations: a simplified cuboid-shape and an anatomical model of an adult male as shown in Fig. 2. The simplified model, originating from [16], has the dimensions of  $480 \text{ mm} \times$

59.5 mm × 44.5 mm and the dielectric properties of skin ( $\epsilon_r = 41.6$ ,  $\sigma = 0.86$  S/m at 915 MHz [26]). The four-term Cole-Cole dielectric relaxation model [25] with the model parameters available from the IT'IS online library [26] was used to model the frequency-dependent dielectric properties of the skin. The skin was selected as the filling material of both models since it is the closest human tissue type to the antenna and its dielectric properties are representative to the whole body. As reported in [16], the inclusion of the internal structures in the anatomical model with their respective dielectric properties, yielded little difference in comparison with a model having homogenous skin filling when modeling a wearable antenna for off-body communications operating at 915 MHz. The antenna optimization was conducted using the cuboid model, because it provided the reduction in the simulation time and mesh size by the factors of 0.77 and 0.7, compared with the anatomical model, respectively. The optimization outcome was finally verified in the anatomical model.

The attainable read range ( $d_{tag}$ ) of the tag is the primary performance indicator for passive UHF RFID tags. It depends on the properties of the tag and reader antennas, the RFID microchip, and the governing emission regulations. For a free space wireless link [8][13]

$$d_{tag} = \frac{\lambda}{4\pi} \sqrt{\frac{\tau \Gamma G EIRP}{P_{ic}}}, \quad \tau = \frac{4Re(Z_a)Re(Z_{ic})}{|Z_a + Z_{ic}|^2}, \quad (1)$$

where  $\lambda$  is the wavelength of the reader's signal,  $\tau$  is the antenna-IC power transfer efficiency determined by the impedance of the tag antenna ( $Z_a$ ) and the RFID microchip ( $Z_{ic}$ ),  $\Gamma$  is the polarization efficiency between the tag antenna and the incident wave,  $G$  is the gain of the tag antenna,  $EIRP$  is the equivalent isotropic radiated power of the reader and  $P_{ic}$  is the turn-on power of the RFID microchip. The polarization efficiency  $0 \leq \Gamma \leq 1$  in (1) is determined by the polarization properties of the tag antenna and the incident wave sent by the reader. The explicit relationship between  $\Gamma$ , axial ratio and the circular polarization ratio are given in Section II.B.

For further assessment, we define the read range coverage  $C_\alpha$  with  $0 < \alpha < 1$ , so that in  $\alpha \cdot 100\%$  of the spatial observation angles  $C_\alpha < d_{tag}(\theta, \phi)$ . This means that when an incident wave from the reader at an unspecified location impinges the tag, there is an  $\alpha \cdot 100\%$  probability for detecting the tag at a distance longer than  $C_\alpha$ . This parameter enables the assessment of the tag's detection reliability in addition to the conventional antenna parameters and the attainable read range. Because we have considered the upper back as the nominal location for the wearable tag, in the further analysis of the spatial coverage, we assume that the reader may be located anywhere behind the person with an equal probability. Thus, we limit the analysis to the spatial directions of a spherical coordinate system centered at the origin in Fig. 2, where  $-90^\circ \leq \theta \leq 90^\circ$  (elevation angle;  $\theta=0$  at z-axis) and  $0^\circ \leq \phi \leq 180^\circ$  (azimuth angle;  $\phi=0$  at x-axis). For computing  $C_\alpha$ , we used the step one degree in formation of the angular grid over the given intervals for  $\theta$  and  $\phi$ .

### B. Experimental Characterization

We patterned the metallic parts of the antenna from copper foil using Summa Cut D60R vinyl plotter and adhered them on the substrate. The RFID microchip was mounted by the

manufacturer on a 3 mm × 3 mm copper fixture patterned on plastic film, which we soldered to the antenna. All the measurements were conducted in an anechoic chamber using Voyantic Tagformance Pro measurement system [28]. For the characterization of fully assembled UHF RFID tags, the system enables the recording of the lowest continuous-wave output power (threshold power:  $P_{th}$ ) of the reader for which the tag under test backscatters a valid 16-bit random number as a response to the reader's query command in ISO 18000-6C communication standard. The attainable read range of the tag, which includes the impact of polarization mismatch between the tag under test and the reader antenna, is estimated from the measured threshold power as

$$d_{tag} = \frac{\lambda}{4\pi} \sqrt{\frac{EIRP P_{th*}}{\Lambda P_{th}}}, \quad (2)$$

where  $P_{th}$  is the measured threshold power of the tag,  $\Lambda$  is a known constant describing the system reference tag's sensitivity, and  $P_{th*}$  is the reference tag's measured threshold power [20]. All the read range results we report in Section IV are measured from the direction z-axis in Fig. 2.

For the assessment of the circular polarization property of the tag, we aligned a linear reader antenna on the z-axis of Fig. 2 with its main beam pointing towards the tag and rotated the reader antenna  $360^\circ$  about the z-axis with a step of  $10^\circ$ . Importantly, by rotating the reader antenna instead of the tag on body during the testing, we capture accurately the axial ratio of the tag while considering the whole body as the antenna platform. In contrast, in [20] we rotated the tag, which may have yielded less accurate results. From the rotation measurement, we extracted the maximum and minimum attainable read ranges  $d_{tag,max}$  and  $d_{tag,min}$ , respectively, over the all the rotation angles. They corresponded with the maximum and minimum polarization efficiencies  $\Gamma_{+LIN}$  and  $\Gamma_{-LIN}$  between the tag antenna and the linear reader antenna, given by

$$\Gamma_{\pm LIN} = \frac{(1 \pm |\gamma_{tag}|)^2}{2(1 + |\gamma_{tag}|^2)}, \quad (3)$$

where  $\gamma_{tag}$  is the circular polarization ratio of the tag antenna [27]. Because  $d_{tag}$  is proportional to the square root of the power received by the tag, we have

$$\frac{\Gamma_{+LIN}}{\Gamma_{-LIN}} = \left( \frac{d_{tag,max}}{d_{tag,min}} \right)^2 = \left( \frac{1 + |\gamma_{tag}|}{1 - |\gamma_{tag}|} \right)^2, \quad (4)$$

where the last equality follows from equation (3). Because the polarization of our antenna is right-handed (reasoning for this is provided in Section IV), we solve  $|\gamma_{tag}|$  from equation (4) under the assumption  $|\gamma_{tag}| > 1$ , and compute the axial ratio and polarization efficiency between the tag and an RHCP reader as

$$A_{tag} = \frac{|\gamma_{tag}| + 1}{|\gamma_{tag}| - 1} \quad \text{and} \quad \Gamma_{RHC} = \frac{1}{1 + |\gamma_{tag}|^{-2}}, \quad (5)$$

respectively [21][27]. With this information, we can estimate the attainable read range of the tag referred to an ideal RHCP reader antenna as

$$d_{tag,RHC} = d_{tag,max} \sqrt{\frac{\Gamma_{RHC}}{\Gamma_{+LIN}}} = d_{tag,min} \sqrt{\frac{\Gamma_{RHC}}{\Gamma_{-LIN}}}, \quad (6)$$

where  $\Gamma_{\pm LIN}$  are computed from equation (3).

### C. Results and Discussion

As shown in Fig. 3 the highest power transfer efficiency of 98%

between the antenna and the IC occurs at 912 MHz and good complex conjugate matching ( $\tau \geq 90\%$ ) is achieved over the frequency range of 908...924 MHz. In terms of the impedance matching, there is little difference between the predictions from the two different simulation models. From the cuboid model,

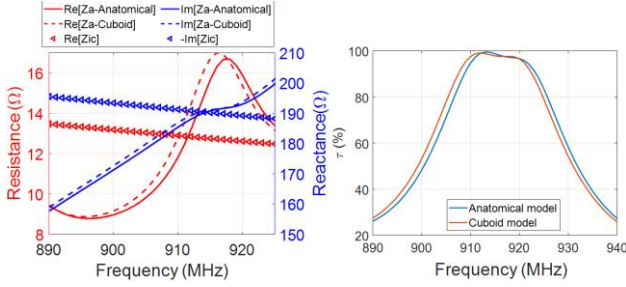


Fig. 3. Simulated antenna impedance and the IC chip impedance (left) and the antenna-IC power transfer efficiency (right).

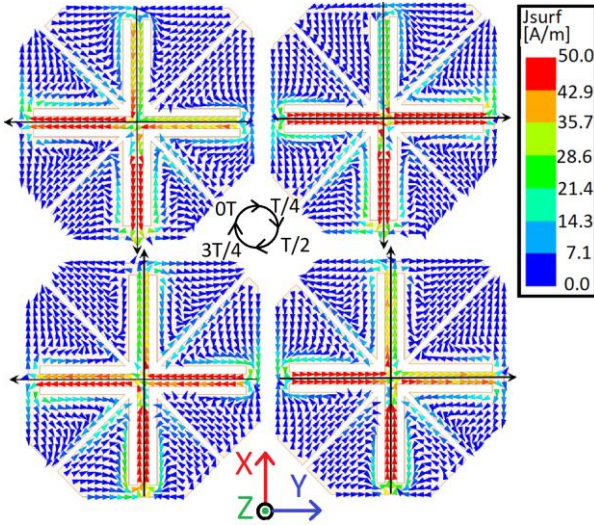


Fig. 4. Simulated surface current density from the cuboid model at different phases of 915 MHz. (a) Phase = 0°. (b) Phase = 90°. (c) Phase = 180°. (d) Phase = 270°.

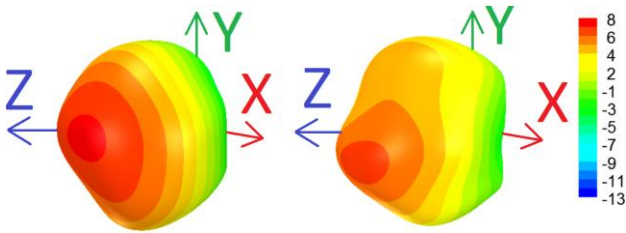


Fig. 5. Simulated 3D RHCP directivity pattern of the antenna from the cuboid model (left) and anatomical model (right) at 915 MHz.

the surface current density distribution of the antenna at the feeding phases of 0°, 90°, 180°, and 270° at 915 MHz is depicted in Fig. 4. The frequency coincides with the lowest axial ratio value. As can be seen, the current vectors at the cross-section in the middle of the antenna are orthogonal, rotating counterclockwise, which indicates right-hand circular polarization in the direction of z-axis [27]. Figure 5 shows the 3D RHCP directivity pattern of the antenna from the two models at 915 MHz. The directivity is high in the direction of z-axis, as desired, with the values of 5.5 dBi and 4.7 dBi from

the cuboid and anatomical models, respectively. However, the peak directivity over all spatial angles occurs approximately at  $\theta = 20^\circ$  and  $\theta = 15^\circ$  in the xz-plane in the cuboid and anatomical models, respectively with the corresponding peak values of 6.7 dBi and 5.4 dBi. The slight offset between the directivity in the direction of z-axis (boresight directivity) and the peak directivity originates from the asymmetrically truncated corners of the radiating patch.

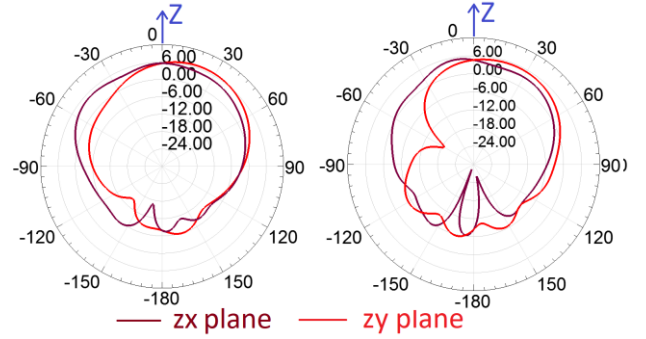


Fig. 6. Simulated (simple model) 2D RHCP directivity with cuboid model (left) and anatomical model (right) at 915 MHz. yz-plane where  $\theta = 0^\circ$  is at z-axis and swept around the yz-plane and xz-plane is plane where  $\theta = 0^\circ$  at z-axis and swept around the xz-plane.

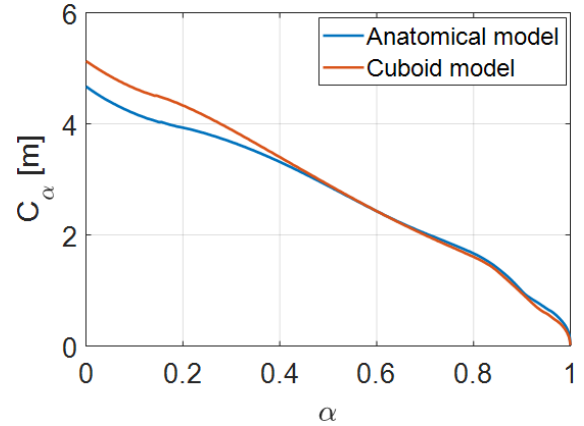


Fig. 7. Spatial coverage of the tag at 915 MHz in the region where  $\theta = -90^\circ \dots 90^\circ$  and  $\phi = 0^\circ \dots 180^\circ$ .

Overall, the 3D RHCP directivity demonstrates wide angular span. In terms of the 2D pattern cuts shown in Fig. 6, the simulated 3 dB beam width of the antenna from the cuboid model is approximately 76° and 118° in xz- and yz-plane, respectively. In comparison, the anatomical model provides the corresponding values of 78° and 81° xz- and yz-plane. The simulated radiation efficiency of the antenna is approximately 4.2% from both models. Overall, the prediction difference between the two models is small in terms of both impedance matching and radiation characteristics.

As shown in Fig. 7, the read range coverage obtained from both models is highly similar especially for  $\alpha \geq 0.4$ . This confirms that both models predict similar radiation properties at the considered observation angles. However, the peak read range which coincides with  $\alpha = 0$ , is slightly higher from the cuboid model. For  $\alpha \geq 0.5$ , both models provide nearly equal spatial coverage and from the value at  $\alpha = 0.5$ , we conclude that there is 50% probability that the tag can be detected from a

distance longer than 2.3 meters with an RHCP reader. This demonstrates good reliability for tag detection in practical scenarios where the alignment between the person and the reader normally varies with the movement of a person wearing the tag.

Finally, to provide further guidelines for tuning the antenna, we conducted the parametric analysis for the shorting pin position (parameter  $e$  in Fig. 1) and the spacing of the L-slots (parameter  $x$  in Fig. 1). While sweeping a particular dimensional parameter, we kept all the other ones fixed to the nominal values listed in Fig. 1. The results are shown in Fig. 8 and Fig. 9. As seen from Fig. 8, as  $x$  increases by 0.4 mm, the optimum axial ratio frequency increases by 37 MHz. At the same time, the frequency of the maximum attainable read range increases. In contrast, Fig. 9 shows that as the parameter  $e$  varies, the axial ratio remains approximately constant whereas notable level-shifts in the attainable read range emerge through the modification of the antenna impedance. Thus, the parameters  $x$  and  $e$  can be used as approximately independent parameters in the post-manufacturing tuning of the antenna to counter the impact of possible modeling uncertainty in the antenna development. As discussed below, we utilized this approach in our experiments.

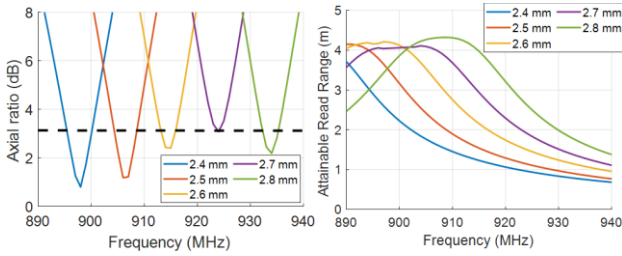


Fig. 8. Simulated (cuboid model) axial ratio and read range of the CP patch tag with various values of the spacing between L-slots (parameter  $x$ )

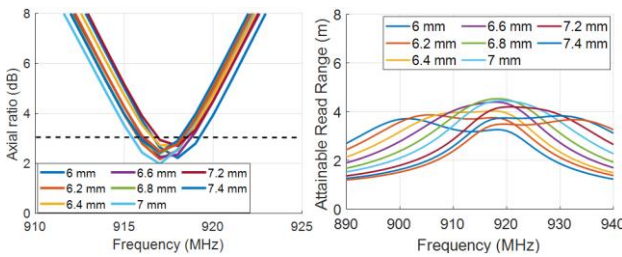


Fig. 9. Simulated (cuboid model) axial ratio and read range of the CP patch tag with various values of the shorting pin position (parameter  $e$  in Fig. 1).

In the experimental characterizations, we attached the tag at various locations on the body on a T-shirt and at the nominal location at the upper back also on a winter coat. As seen from the results in Fig. 10, in the measurement of the initial sample shows a downwards shift in frequency compared with the simulations. We expect this to originate primarily from the approximations involved in the simulation models. Therefore, we applied the post-manufacturing tuning to bring the axial ratio minimum frequency closer to the targeted 915 MHz. This was achieved by changing the spacing of the L-slots from  $x = 2.6$  mm to  $x = 3$  mm. The tuned sample provided the axial ratio value of 2.1 dB at 917 MHz when it was worn at the nominal location in the upper back. Among all the tested locations, the

maximum frequency-shift in the axial ratio was only 5 MHz and, in all cases, the minimum frequency remained within the UHF RFID band (902...928 MHz). Moreover, in all cases the minimum value of the axial ratio was approximately 2 dB.

The numerically predicted and measured attainable read range of the tag is shown in Fig. 11. From the simulations, the peak read range is between 4.5 m and 5.1 m and from the direction z-axis (see Fig. 2) between 4 m and 4.5 m. The measured value from the direction of z-axis was 5.8 meters when the tag was attached to the upper back of a person on a T-shirt and it ranged between 5.5 m and 6 meters in the four different body-worn configurations. This verifies that even though the upper back was considered the nominal location of the tag when the antenna was optimized using the numerical body models, in practice, it maintains stable performance at various other locations on body. This is of major importance for practical applications.

When the reader antenna is linearly polarized, the attainable read range varies depending on the mutual rotation angle between the reader and the tag antennas. In this case, we can characterize the tag in terms of its minimum and maximum  $d_{tag}$

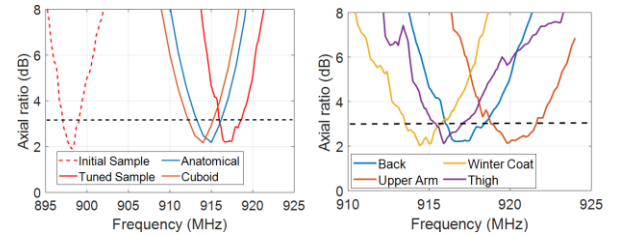


Fig. 10. Axial ratio of the tag antenna when the tag is attached to person's back (left) and at different parts of the body (right). The figure on the right contains only measured results.

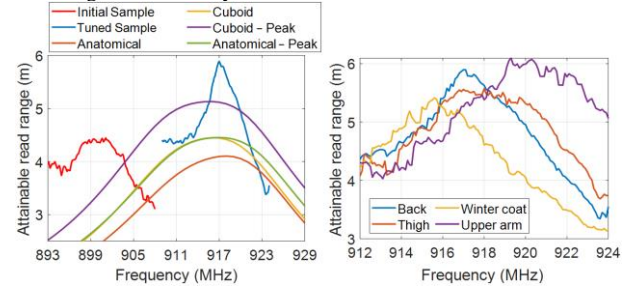


Fig. 11. The attainable read range of the tag when the reader antenna is RHCP and the tag is attached to person's back (left) and at different parts of the body (right). The figure on the right contains only measured results.

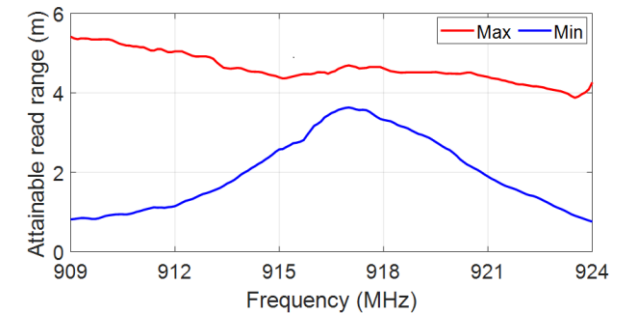


Fig. 12. The measured attainable read range of the tag (tuned sample) when it is attached to a person's back and the reader antenna is linearly polarized.

at each frequency, corresponding with the minimum ( $\Gamma_{-LIN}$ ) and maximum ( $\Gamma_{+LIN}$ ) polarization efficiency. As shown in Fig. 12, in this case  $d_{tag}$  varies between 3.8 m and to 4.5 m at the axial ratio minimum frequency, depending on the antennas' mutual rotation angle. This means that despite being circularly polarized, the tag can yet be detected at reasonable distance in an RFID system where linearly polarized reader antennas were deployed.

Finally, our proposed tag is compared with previous works on circularly polarized passive UHF RFID tags in Table I. As can be seen, the tag antenna gain, and the tag read range from research [30] and [32] is notably high in comparison with other works. However, also the size of the tag in these works is large, making it only wearable at the front or back of the torso. The circular footprint of the tag from research [31] is comparable with our proposed tag, but as a single-layered antenna without a ground plane, its performance is limited by the antenna-body coupling. Overall, compared with the previous works, our tag strikes a favorable balance between the size and performance and is small enough to be worn at various locations on body.

TABLE I  
COMPARISON WITH THE CONTEMPORARY RESEARCH WORK.

Ref.	Antenna type	3-dB AR BW (MHz)	Read range (m)	Gain (dBi)	Antenna size (mm)
[29]	Patch	6	2.8	-7	70 × 70 × 1.6
[20]	Dipole on AMC	40	15.7	5	215 × 215 × 6
[31]	Split ring	23	2	-9.6	$\pi \times 22^2 \times 3$
[32]	Patch	6	8.5	N/A	149.5 × 148 × 5
This work	Patch	3	5.8	-7.1	50 × 50 × 4.5

### III. CONCLUSION

Wearable antennas are the core technology for modern wireless body-area systems that enable important future applications. We presented a circularly polarized antenna for wearable passive UHF RFID tags. It features a low axial ratio value in various body-worn configurations and has a small size of 5-by-5 cm on a low-permittivity textile substrate that enables seamless cloth-integration. Simultaneously with the CP radiation, the antenna geometry provides good complex conjugate impedance matching between the antenna and an RFID integrated circuit that exhibits low-resistance and capacitive impedance similar with many RF energy harvesting systems. Numerical simulations showed that the wearable tag antenna provides a broad radiation beam with the peak directivity of over 5 dBi which enables good detection reliability of the tag also when the user is not perfectly aligned with the reader. The peak of measured attainable read range of the implemented tag was 5.8 meters with an RHCP reader antenna and ranged between 3.8 m and 4.5 m for a linearly polarized reader antenna.

### REFERENCES

[1] P. Van Daele, I. Moerman, and P. Demeester, "Wireless body area networks: status and opportunities," in *URSI General Assembly and Scientific Symposium*, Beijing, China, Aug. 2014, 4 pages.

[2] Y.-L. Zheng, X.-R. Ding, C. C. Y. Poon, B. P. L. Lo, H. Zhang, X.-L. Zhou, G.-Z. Yang, N. Zhao, and Y.-T. Zhang, "Unobtrusive sensing and wearable devices for health informatics," *IEEE Trans. Biomed. Eng.*, vol. 61, no. 5, pp. 1538–1554, May 2014.

[3] S. Movassaghi, M. Abolhasan, J. Lipman, D. Smith, and A. Jamalipour, "Wireless body area networks: a survey," *IEEE Commun. Surveys Tuts.*, vol. 16, no. 3, pp. 1658–1686, Jan. 2014.

[4] A. Sani, M. Rajab, R. Forster, and Y. Hao, "Antennas and propagation of implanted RFIDs for pervasive healthcare applications," *Proc. IEEE*, vol. 98, no. 9, pp. 1648–1655, Sep. 2010.

[5] J. Grosinger, "Feasibility of backscatter RFID system on the human body," *EURASIP J. Embedded Syst.*, vol. 2013, no. 2, 10 pages, Mar. 2013.

[6] W. Mongan, E. Anday, G. Dion, A. Fontecchio, K. Joyce, T. Kurzweg, Y. Liu, O. Montgomery, I. Rasheed, C. Sahin, S. Vora, and K. Dandekar, "A multi-disciplinary framework for continuous biomedical monitoring using low-power passive RFID-based wireless wearable sensors," in *IEEE International Conference on Smart Computing*, St. Louis, MO, USA, May 2016, 6 pages.

[7] S. Milici, S. Amendola, and A. Bianco, "Epidermal RFID passive sensor for body temperature measurements," in *IEEE RFID technology and applications conference (RFID-TA)*, Tampere, Finland, Sep. 2014, pp. 140–144.

[8] P. V. Nikitin, "Antennas and propagation in UHF RFID systems," in *IEEE International Conference on RFID*, Las Vegas, NV, USA, Apr. 2008, pp. 277–288.

[9] H. H. Tran, S. X. Ta, and I. Park, "A compact circularly polarized crossed-dipole antenna for an RFID tag," *IEEE Antennas Wireless Propag. Lett.*, vol. 14, pp. 674–677, Dec. 2010.

[10] H. D. Chen, C. H. Tsai, and C. Y. Kuo, "Circularly polarized loop tag antenna for long reading range RFID applications," *IEEE Antennas Wireless Propag. Lett.*, vol. 12, pp. 1460–1463, Nov. 2013.

[11] J. H. Lu and B. S. Chang, "Planar compact square-ring tag antenna with circular polarization for UHF RFID applications," *IEEE Trans. Antennas Propag.*, vol. 65, no. 2, pp. 432–441, Nov. 2016.

[12] A. S. M. Sayem, D. Le, R. B. V. B. Simorangir, T. Björninen, K. P. Esselle, R. M. Hasmi, and M. Zhadobov, "Optically transparent flexible robust circularly polarized antenna for UHF RFID tags," *IEEE Antennas Wireless Propag. Lett.*, vol. 19, no. 12, pp. 2334–2338.

[13] G. Marrocco, "The art of UHF RFID antenna design: impedance-matching and size-reduction techniques," *IEEE Antennas Propag. Mag.*, vol. 50, no. 1, pp. 66–79, Mar. 2008.

[14] E. Perret, S. Tedjini, and R. S. Nair, "Design of antennas for UHF RFID tags," *Proc. IEEE*, vol. 100, no. 7, pp. 2330–2340, July 2012.

[15] T. Mäkinen and T. Kellomäki, "Body effects on thin single-layer slot, self-complementary, and wire antennas," *IEEE Trans. Antennas Propag.*, vol. 62, no. 1, pp. 385–392, Nov. 2013.

[16] T. Björninen, "Comparison of three body models of different complexities in modelling of equal-sized dipole and folded dipole wearable passive UHF RFID tags," *Appl. Computational Electromagn. Soc. J.*, vol. 33, no. 6, pp. 706–709, May. 2018.

[17] E. K. Kaivanto, M. Berg, E. Salonen, and P. de Maagt, "Wearable circularly polarized antenna for personal satellite communication and navigation," *IEEE Trans. Antennas Propag.*, vol. 59, no. 12, pp. 4490–4496, Dec. 2011.

[18] M. Joler and M. Boljkovac, "A sleeve-badge circularly polarized textile antenna," *IEEE Trans. Antennas Propag.*, vol. 66, no. 3, pp. 1576–1579, Mar. 2018.

[19] J. Li, Y. Jiang, and X. Zhao, "Circularly polarized wearable antenna based on NinjaFlex-embedded conductive fabric," *Intl. J. Antennas Propag.*, vol. 2019, article ID 3059480, 8 pages, Sep. 2019.

[20] C. W. Chiu and J. H. Hong, "Circularly polarized tag antenna on an AMC substrate for wearable UHF RFID applications," in *IEEE-APS Topical Conference on Antennas and Propagation in Wireless Communications*, Verona, Italy, Sep. 2017, pp. 71–74.

[21] D. Le, L. Ukkonen, and T. Björninen, "Circularly polarized corner-truncated and slotted microstrip patch antenna on textile substrate for wearable passive UHF RFID tags," in *European Conference on Antennas and Propagation*, Copenhagen, Denmark, Mar. 2020, 5 pages.

[22] T. Björninen, L. Sydänheimo, and L. Ukkonen, "Development and validation of an equivalent circuit model for UHF RFID IC based on

- wireless tag measurements,” in *Antenna Measurement Techniques Association Symposium*, Bellevue, WA, USA, Oct. 2012, pp. 21–26.
- [23] T. Ali and R. C. Biradar, “A miniaturized circularly polarized coaxial fed superstrate slot antenna for L-band application,” *Internet Technol. Lett.*, vol. 6, no. 1, 7 pages, Nov. 2018.
- [24] D. Le, Y. Kuang, L. Ukkonen, and T. Björninen, “Microstrip transmission line model fitting approach for characterization of textile materials as dielectrics and conductors for wearable electronics,” *Intl. J. Numerical Modelling Electronic Netw. Dev. Fields*, vol. 32, no. 6, 10 pages, Feb. 2019.
- [25] S. Gabriel, R. W. Lau, and C. Gabriel, “The dielectric properties of biological tissues: III. Parametric models for the dielectric spectrum of tissues,” *Phys. Med. Biol.*, vol. 41, no. 11, pp. 2271–2293, Nov. 1996.
- [26] IT’IS Foundation, Tissue Properties [Online]. Available: <https://www.itis.ethz.ch/virtual-population/tissue-properties/downloads>
- [27] Thomas A. Milligan, *Modern Antenna Design*, 2nd ed., vol. 2. John-Wiley & Sons, Inc., pp. 18–24.
- [28] Voyantic, Ltd., Espoo, Finland: <http://www.voyantic.com/>
- [29] H. D. Chen, W. S. Chen, and S. H. Kuo, “CP RFID tag design for metal surface mount,” in *Cross Strait Quad-Regional Radio Science and Wireless Technology Conference*, Harbin, China, July 2011, pp. 491–493.
- [30] S. Ma, L. Ukkonen, L. Sydänheimo, and T. Björninen, “Dual-Layer circularly polarized split ring resonator inspired antenna for wearable UHF RFID tag,” in *IEEE International Symposium on Antennas and Propagation*, Boston, MA, USA, July 2018, pp. 683–684.
- [31] Y. Kuang, S. Ma, L. Ukkonen, J. Virkki, and T. Björninen, “Circularly polarized textile tag antenna for wearable passive UHF RFID systems”, in *International Applied Computational Electromagnetics Society Symposium-China*, Beijing, China, July 2018, 2 pages.